Korean J. Chem. Eng., 32(5), 993-1000 (2015)
DOI: 10.1007/s11814-014-0275-0

pISSN: 0256-1115
eISSN: 1975-7220

Thiazole derivatives as efficient corrosion inhibitor for oil-well tubular steel in hydrochloric acid solution

Mahendra Yadav†, Dipti Sharma, and Sumit Kumar

Department of Applied Chemistry, Indian School of Mines, Dhanbad 826004, India
(*Received 26 June 2014 • accepted 11 September 2014*)

Abstract−The effect of 1-(benzo[d]thiazol-2-yl)-3-chloro-4-(3,5-dichlorophenyl)-4-methylazetidin-2-one (BDMA) and 3-(benzo[d]thiazol-2-yl)-2-(3,5-dichlorophenyl)-2,5-dimethylthiazolidin-4-one (BDMT) on the corrosion of oil well tubular steel (N80 steel) in 15% hydrochloric acid solution was investigated by means of potentiodynamic polarization and electrochemical impedance spectroscopy (EIS) techniques. The surface morphology of the uninhibited and inhibited samples was studied with atomic force microscopy (AFM). The corrosion inhibition efficiency of both inhibitors increased with increasing inhibitors concentration. The adsorption of both inhibitor molecules on surface of N80 steel obeys Langmuir adsorption isotherm. Potentiodynamic polarization measurements indicated that both the studied inhibitors act as mixed type inhibitor. Quantum chemical calculations were carried out using density functional theory (DFT) to correlate the experimental results with the theoretical results.

Keywords: N80 Steel, Hydrochloric Acid, Corrosion Inhibition, EIS, AFM, Density Functional Theory

INTRODUCTION

The economic impact of corrosion is incredibly large and significantly affects the economy of the country and especially of the industry. The need to use constructional material safely, cost effectively and with due attention towards the complications arising from their corrosion is a primary consideration in many industries. From the viewpoint of a nation's economy, it is very necessary to adopt appropriate ways and means to reduce the losses due to corrosion. With technological and industrial growth, the use of metals and alloys is increasing rapidly, and any step in the direction of preventing corrosion to a reasonable extent would be of great help. Acidizing of oil well through N80 steel tubes is a frequently used stimulation technique for increasing crude oil productivity by enlarging the microscopic flow channel. In petroleum industry 15% hydrochloric acid is used for the acidizing treatment because it is commercially available, cost effective and leaves no insoluble reaction product. Because of the aggressiveness of hydrochloric acid solutions, N80 steel tubing corrodes severely during this process, which results in terrible waste of both resources and money. A corrosion inhibitor is often added in the acid solution to mitigate the corrosion of the tubing material by acid attack. Use of inhibitors is one of the most widespread and cost-effective measures to combat corrosion of metals. Most of the inhibitors for corrosion of N80 steel in acidic medium are organic compounds containing nitrogen, oxygen and/or sulfur atoms [1,2]. The adsorption of the inhibitor on the metal surface is a complex mechanism involving a number of factors such as the nature of the metal, the environment, the electrochemical potential at the metal interface and nature of the inhibitor [3]. Compounds that contain both nitrogen and sulfur are of particular importance since these provide an excellent inhibition in comparison with the compounds containing either sulfur or nitrogen [4,5]. Both the studied compounds contain benzothiazole ring. Benzothiazole is a fused heterocyclic molecule that has strong ability of bonding with metal ions via donor atoms (N and S) to form metal complexes. Benzothiazole molecule shows three anchoring sites suitable for surface bonding: the nitrogen atom with its lone pair of electrons, sulfur atom and the aromatic rings [6,7]. Thus, it is expected that both the studied compounds will show good corrosion inhibition efficiencies.

The aim of this work was to synthesize and characterize benzothiazole derivatives namely, 1-(benzo[d]thiazol-2-yl)-3-chloro-4-(3,5-dichlorophenyl)-4-methylazetidin-2-one (BDMA) and 3-(benzo[d]thiazol-2-yl)-2-(3,5-dichlorophenyl)-2,5-dimethylthiazolidin-4-one (BDMT), and to study their corrosion inhibition behavior against corrosion of oil well tubular steel (N80 steel) in 15% HCl solution by means of potentiodynamic polarization, electrochemical impedance spectroscopy and quantum chemical calculations.

EXPERIMENTAL PROCEDURE

1. Materials

1-1. N80 Steel Sample

Electrochemical studies were carried out on N80 steel samples having the composition (wt%): C, 0.31; Mn, 0.92; Si, 0.19; S, 0.008; P, 0.010; Cr, 0.20 and Fe in balance. The surface preparation of the N80 steel specimens with size 1.0 cm×1 cm×0.1 cm, with an exposed area of 1 cm^2 (rest covered with araldite resin) with 3 cm long stem, was carried out using abrasive papers (120, 220, 400, 600, 800, 1,500 and 2,000 grade) for electrochemical measurements. Specimens were washed with distilled water, degreased with acetone and desiccated at ambient temperature prior to use.

†To whom correspondence should be addressed.
E-mail: yadav_drmahendra@yahoo.co.in

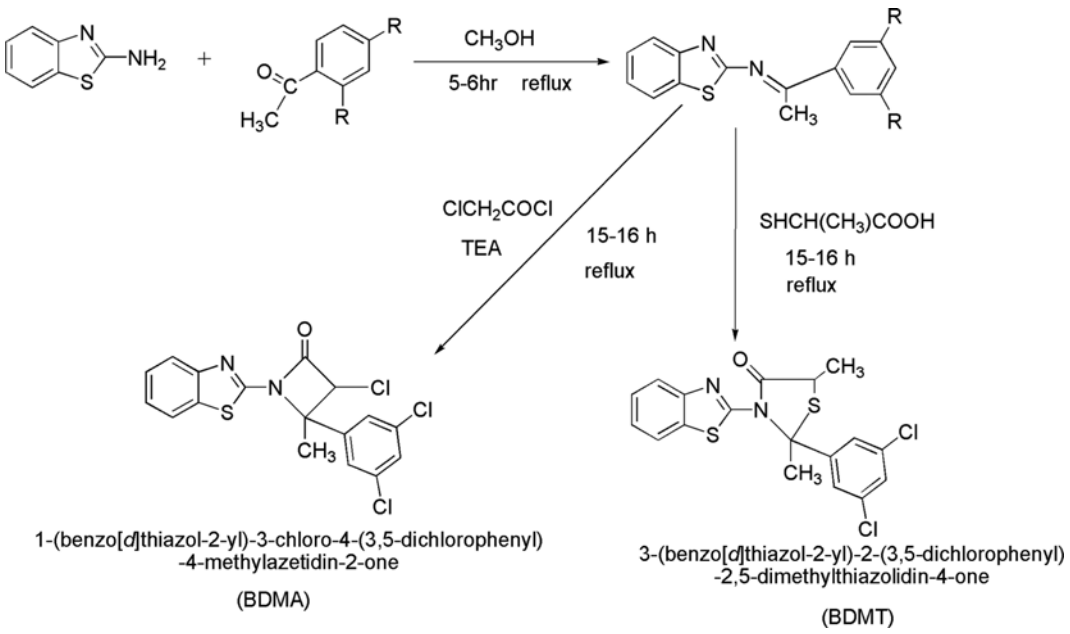

Scheme 1. Synthetic route and structures of BDMA and BDMT.

1-2. Test Solutions

Experiments were performed in 15% HCl solution which was prepared in double distilled water using AR grade hydrochloric acid supplied by Ranbaxy fine chemicals. For potentiodynamic polarization and AC impedance studies, the test solution used was 250 mL. The concentration of inhibitors by weight in 15% HCl solution ranged from 10 ppm to 50 ppm.

1-3. Synthesis of Corrosion Inhibitor

The compounds BDMA and BDMT were synthesized in laboratory as per the reported procedure [8] as given in Scheme 1. The purity of the synthesized compounds was checked by thin layer chromatography (TLC).

Physico - chemical and spectroscopic data of synthesized compounds are given below:

1-3-1. BDMA

Yield: 64%; m.p.: 162; Elemental analysis (%): Calculated for $C_{17}H_{11}N_2OSCl_3$; C, 51.32; H, 2.76; N, 7.04%. Found: C, 51.16; H, 2.74; N, 7.12%.

IR (KBr) (cm^{-1}): 1535 (C=N), 1550 (C=C aromatic), 3120 (C-H aromatic), 2940 (C-H, aliphatic), 1620 (C=O), 670 (C-S).

1-3-2. BDMT

Yield: 67%; m.p.: 154; Elemental analysis (%): Calculated for $C_{18}H_{14}N_2OS_2Cl_2$; C, 52.81; H, 3.42; N, 6.84%. Found: C, 52.62; H, 3.34; N, 6.48%.

IR (KBr) (cm^{-1}): 1660 (C=N), 1540 (C=C aromatic), 3130 (C-H aromatic), 2920 (C-H, aliphatic), 1640 (C=O), 680 (C-S).

2. Methods

2-1. Electrochemical Studies

Polarization and electrochemical impedance spectroscopy measurements were conducted in a conventional three-electrode cell consisting of N80 steel sample of 1 cm^2 exposed area as working electrode, a platinum counter electrode and a saturated calomel electrode (SCE) as reference electrode, using CH electrochemical workstation (Model No: CHI 760D, manufactured by CH Instruments, Austin, USA) at 303 K. Prior to polarization and impedance measurements, the working electrode was immersed for 1 hour in the test solution until a steady-state of the open-circuit potential was obtained. Potentiodynamic polarization curves were obtained at the scan rate of 1.0 mVs^{-1} in the potential range from +300 to −300 mV vs SCE with respect to open circuit potential. Corrosion current density (i_{corr}) was obtained by Tafel extrapolation method.

Electrochemical impedance measurements were carried out using AC signals of amplitude 10 mV peak to peak at the open circuit potential in the frequency range 100 kHz to 10 mHz. All impedance data were fitted to appropriate equivalent circuits using ZSimpWin.3.21 software.

2-2. Atomic Force Microscopy

The AFM images of polished, uninhibited and inhibited N80 steel samples were taken with a Nanosurf Easyscan2 instrument, Model: NT-MDT, Russia; Solver Pro-47.

2-3. Quantum Chemical Study

Complete geometrical optimizations of the investigated molecules were performed using density functional theory with the Beck's three parameter exchange functional along with the Lee-Yang-Parr nonlocal correlation functional (B3LYP) with 6-31G (d, p) basis set was implemented in Gaussian 03 program package [9]. Theoretical parameters such as the energies of the highest occupied and lowest unoccupied molecular orbital (E_{HOMO} and E_{LUMO}), energy gap (ΔE) and dipole moment (μ) were determined.

RESULTS AND DISCUSSION

1. Potentiodynamic Polarization Measurements

The effect of addition of inhibitors (BDMA and BDMT) on the anodic and cathodic polarization curves for N80 steel in 15% HCl solution was studied and polarization curves are shown in Fig. 1(a),

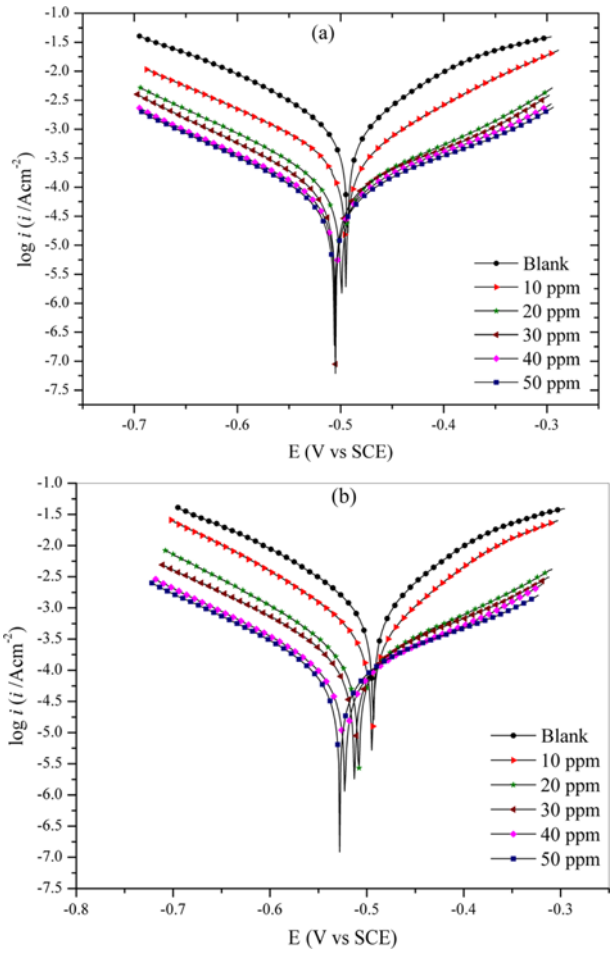

Fig. 1. Potentiodynamic polarization curves for N80 steel in 15% HCl solution in the presence and absence of inhibitor at 303 K. (a) BDMT (b) BDMA.

(b) at 303 K. The corrosion current densities were calculated by Tafel extrapolation method. The corrosion parameters such as corrosion potential (E_{corr}), anodic Tafel slope (β_a), cathodic Tafel slope (β_c), corrosion current density (i_{corr}) and percentage inhibition efficiency (η %) obtained from these curves are given in Table 1. The percentage inhibition efficiency and surface coverage (θ) was calculated using the equations given below:

$$\eta(\%) = \frac{i^0_{corr} - i_{corr}}{i^0_{corr}} \times 100 \quad (1)$$

$$\theta = 1 - \frac{i_{corr}}{i^0_{corr}} \quad (2)$$

where, i^0_{corr} and i_{corr} are the values of corrosion current density in absence and presence of inhibitors, respectively.

It is clear from the Fig. 1(a), (b) that both the anodic metal dissolution and cathodic hydrogen evolution curves were shifted towards the lower current density after the addition of inhibitors to the aggressive medium. The shift of these curves towards lower current density was more pronounced with the increasing inhibitor concentration. These results indicate that both the studied inhibitors act as the mixed type corrosion inhibitor. The inhibitor molecules adsorb

Table 2. Adsorption parameters for studied inhibitors calculated from different adsorption isotherm for N80 steel in 15% HCl solution at 303 K

Adsorption isotherm	Inhibitor	Correlation coefficient	Slope	K_{ads} (M^{-1})
Temkin	BDMT	0.932	0.37	3.8×10^{-3}
	BDMA	0.938	0.36	4.1×10^{-3}
Frumkin	BDMT	0.936	0.65	3.2×10^{-9}
	BDMA	0.947	0.57	7.9×10^{-9}
Flory & Huggins	BDMT	0.958	1.40	1.7×10^{-7}
	BDMA	0.940	1.24	2.6×10^{-6}
Langmuir	BDMT	0.999	0.99	5.4×10^{4}
	BDMA	0.998	0.98	1.1×10^{4}

Table 1. Corrosion parameters for N80 steel in 15% HCl solution in the absence and presence of different concentrations of inhibitors at 303 K

Conc. (ppm)	Tafel extrapolation data					EIS data					
	E_{corr} (V vs SCE)	β_a (mV dec^{-1})	$-\beta_c$ (mV dec^{-1})	I_{corr} (μA cm^{-2})	η %	R_s (Ω cm^2)	R_{ct} (Ω cm^2)	Y_0 (μF cm^{-2})	n	C_{dl} (μF cm^2)	η %
Blank BDMT	−495	93	142	568	-	0.93	20	573	0.845	252	-
10	−504	98	154	162	71.5	0.62	66	184	0.871	96	69.7
20	−508	91	136	82	84.6	0.57	138	126	0.882	72	85.5
30	−510	84	144	48	91.5	0.75	206	95	0.886	58	90.3
40	−515	76	162	28	95.1	0.54	340	55	0.915	38	94.1
50	−522	88	171	22	96.1	0.57	432	32	0.936	24	95.4
BDMA											
10	−497	96	131	178	68.7	0.73	58	207	0.867	106	65.5
20	−498	74	152	88	84.5	0.84	122	151	0.877	85	83.6
30	−502	78	162	67	88.2	0.93	188	105	0.893	66	89.3
40	−505	86	124	48	91.5	0.66	260	72	0.907	47	92.3
50	−508	92	146	39	93.1	0.64	320	48	0.923	33	93.7

on the N80 steel surface and blocking the available reaction sites [10]. It is clear from Table 2 that the slopes of the cathodic (β_c) and anodic (β_a) Tafel lines are approximately constant and independent of inhibitor concentration. These results indicate that there is no major change in corrosion mechanism of N80 steel in 15% HCl solution in absence and presence of studied inhibitors and these inhibitors act by simply blocking the active sites at the N80 steel surface and decrease the surface area for corrosion process. The presence of inhibitor cause minor change in E_{corr} values with respect to the E_{corr} value in absence of inhibitor. It is reported that if the change in E_{corr} value in presence of inhibitor with respect to the E_{corr} value in absence of inhibitor is more than 85 mV, the inhibitor is recognized as an anodic or a cathodic type inhibitor, whereas if the change in E_{corr} value is less than 85 mV, the inhibitor is recognized as mixed type inhibitor [11]. The maximum displacement in present study is 27 mV, which is less than 85 mV/SCE, indicated that BDMA and BDMT act as mixed type inhibitor affecting both anodic and cathodic reactions.

2. Electrochemical Impedance Spectroscopy (EIS)

EIS measurements were performed to determine the impedance parameters of the N80 steel/hydrochloric acid interface in the absence and presence of various concentrations of inhibitors. The Nyquist and Bode plots for N80 steel obtained at interface in 15% HCl solution with and without the different concentrations of BDMT and BDMA at 303 K are shown in Fig. 2(a), (b) and Fig. 4(a), (b), respectively. The Nyquist plots in absence and presence of inhibitors are characterized by one capacitive loop. The capacitive loops are not perfect semicircles, because of non-ideal structure of the metal/solution interface [12-14]. Therefore, a constant phase element (CPE) was introduced in the equivalent circuit instead of a pure double layer capacitor (C_{dl}) to give more accurate fit of experimental data.

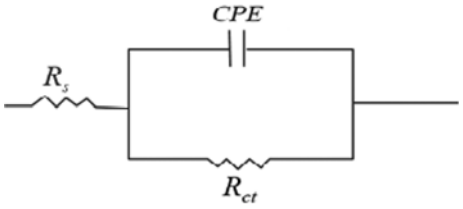

Fig. 3. Equivalent circuit applied for fitting of the impedance spectra.

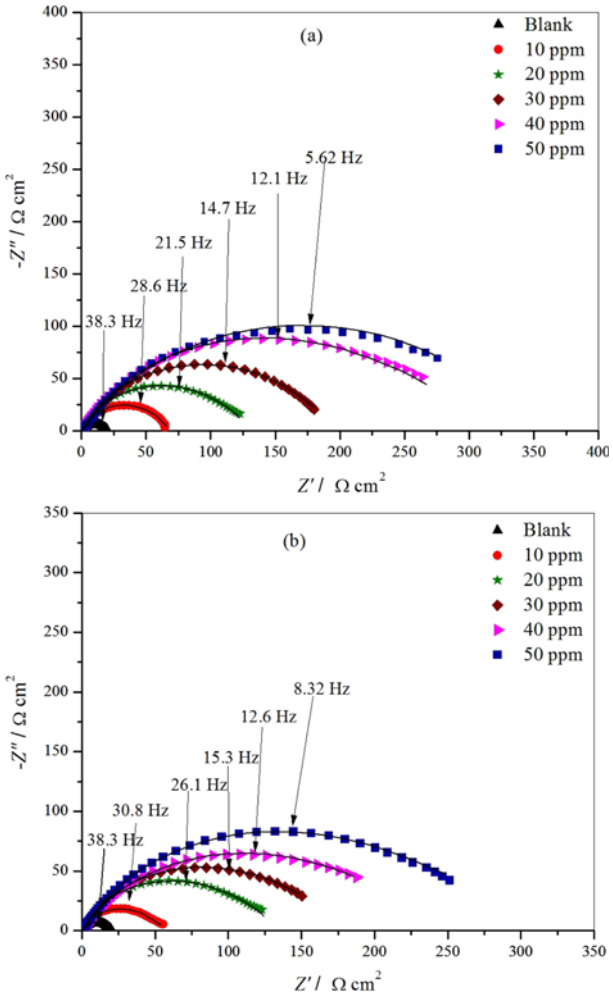

Fig. 2. Nyquist plot for N80 steel in 15% HCl solution in the presence and absence of inhibitor, symbols for experimental data and solid line for fitting values, at 303 K (a) BDMT (b) BDMA.

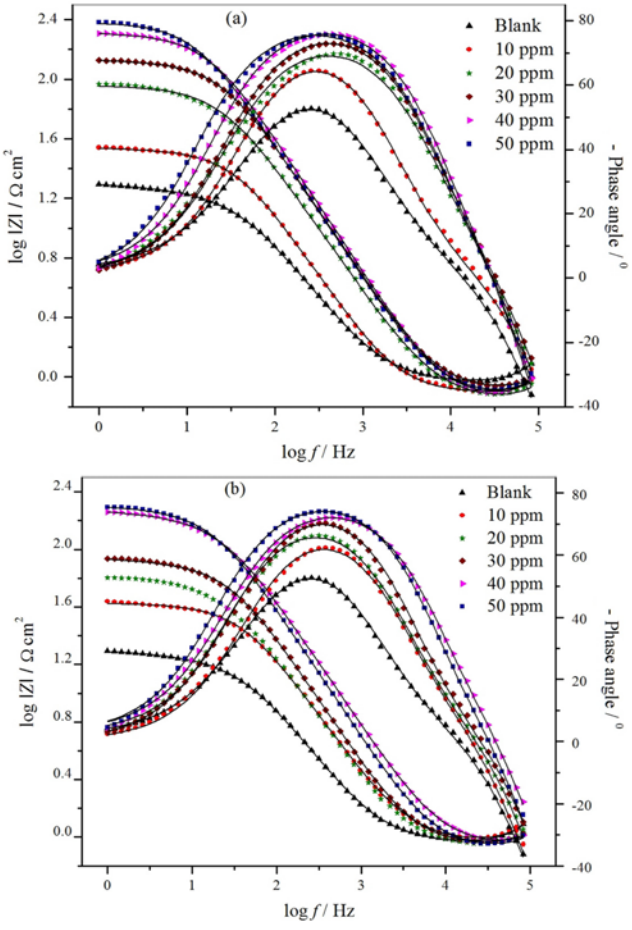

Fig. 4. Bode (log f vs log|Z|) and phase angle (log f vs -phase) plots of impedance spectra for N80 steel in 15% HCl solution in the presence and absence of inhibitor, symbols for experimental data and solid line for fitting values, at 303 K (a) BDMT (b) BDMA.

The impedance function of a CPE is defined by

$$Z_{CPE}=[Y_0 (j\omega)^n]^{-1} \quad (3)$$

where Y_0 is the magnitude of the CPE, n the CPE exponent, j is the imaginary number ($j^2=-1$) and ω is the angular frequency ($\omega=2\pi f_{max}$) for which imaginary component of impedance is maximum. When the value of n is 1, the CPE behaves like an ideal double-layer capacitance (C_{dl}).

The difference in real impedance at lower and higher frequencies is considered as the polarization resistance (R_p) which contains charge transfer resistance (R_{ct}), double layer resistance (R_d), accumulation resistance (R_a) and film resistance (R_f) at the metal/solution interface [15,16]. The EIS spectra of all tests were analyzed by using the equivalent circuit shown in Fig. 3, which is a parallel combination of the R_{ct} and CPE, both in series with the solution resistance (R_s). This type of electrochemical equivalent circuit was reported previously to model the iron/acid interface [13].

The electrochemical impedance data such as R_s, R_{ct}, and CPE constants (Y_0 and n) obtained from fitted spectra are listed in Table 1. The inhibition efficiency was calculated from charge transfer resistance values obtained from impedance measurements using the following relation:

$$\eta(\%)=\frac{R_{ct(inh)}-R_{ct}}{R_{ct(inh)}}\times 100 \quad (4)$$

where $R_{ct(inh)}$ and R_{ct} are charge transfer resistance in presence and absence of inhibitor respectively.

The values of C_{dl} were calculated from charge transfer resistance and CPE constants using the expression [17]

$$C_{dl}=(Y_0 R_{ct}^{1-n})^{1/n} \quad (5)$$

The value of n represents the deviation from the ideal behavior and it lies between 0 and 1.

The data shown in Table 1 reveal that the values of R_{ct} increase with addition of inhibitors as compared to the blank solution. The increase in R_{ct} values is attributed to the formation of a protective film at the metal/solution interface [18]. The C_{dl} value decreased with increasing the concentration of inhibitors. The decrease in C_{dl}, which is the result of a decrease in local dielectric constant and/or an increase in the thickness of the electrical double layer, suggests that the inhibitor molecules act by adsorption at the metal/solution interface [19].

The Bode phase angle plots (Fig. 4(a), (b)) show single maximum (one time constant) at intermediate frequencies, broadening of this maximum in presence of inhibitors accounts for the formation of a protective layer on the electrode surface. The higher values of phase angle for inhibited solution than uninhibited solution reflect the inhibitive action of inhibitors. Fig. 4(a), (b) shows that the impedance value in the presence of both inhibitors is larger than in absence

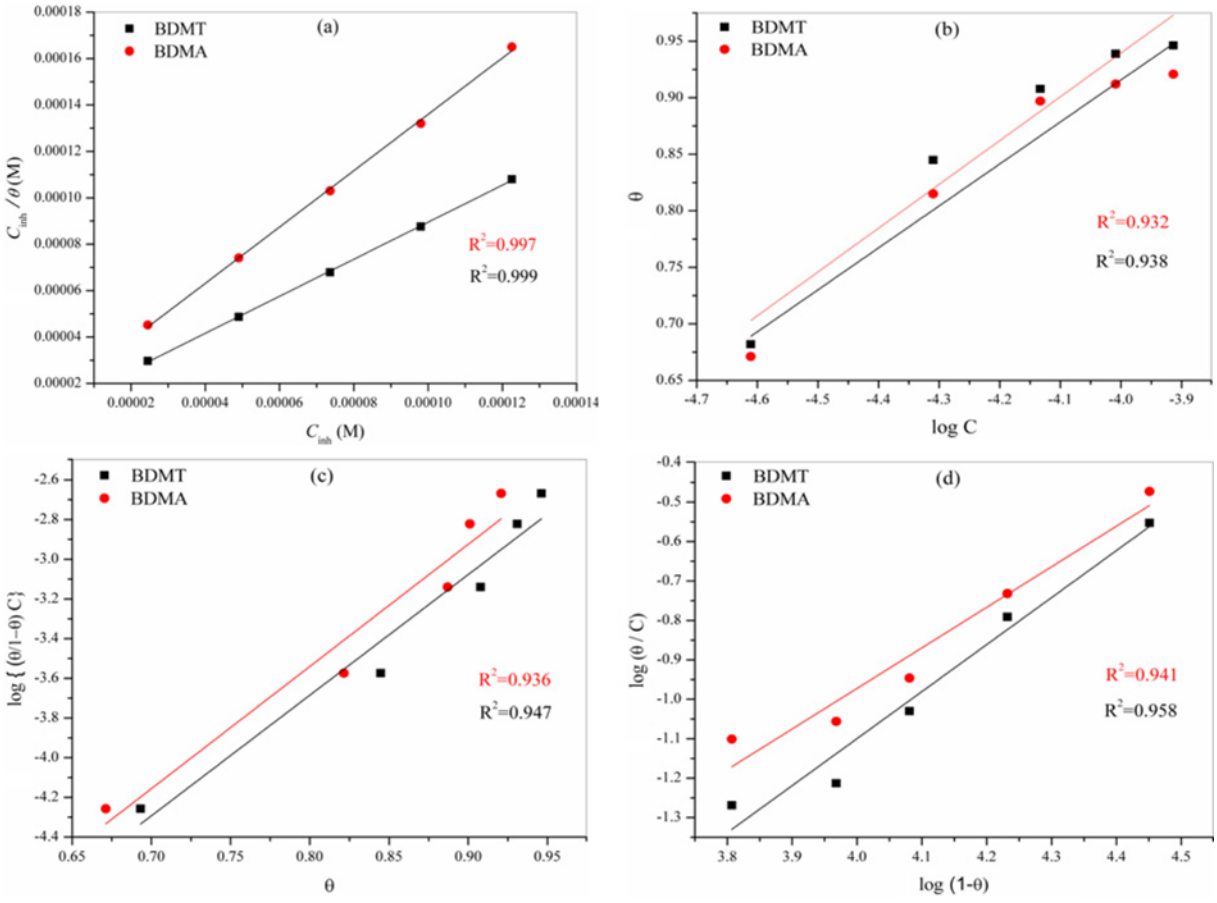

Fig. 5. Adsorption isotherms (a) Langmuir, (b) Temkin, (c) Frumkin, (d) Flory-Huggins.

of inhibitors and the value of impedance increases on increasing the concentration of both studied inhibitors. These indicate that the corrosion rate is reduced in presence of the inhibitors and continued to decreasing on increasing the concentration of inhibitors.

3. Adsorption Isotherm

The adsorption process is influenced by chemical structure of organic compound, the distribution of charge in molecule, the nature and surface charge of metal and the type of aggressive media. To clarify the nature and the strength of the adsorption of BDMA and BDMT on N80 steel, the experimental results were fitted to Langmuir, Temkin, Frumkin and Flory-Huggins adsorption isotherms, as shown in Fig. 5(a), (b), (c), (d)). The correlation coefficient (R^2) and slope values of these plots are given in Table 2. The correlation coefficient (R^2) and slope values in case of Langmuir adsorption isotherm show least deviation from unity as compared to other adsorption isotherms. Thus, adsorption of BDMA and BDMT obey the Langmuir adsorption isotherm represented by the following equation:

$$\frac{C_{inh}}{\theta} = \frac{1}{K_{ads}} + C_{inh} \quad (6)$$

where, C_{inh} is the inhibitor concentration, K_{ads} is the equilibrium constant for adsorption-desorption process.

The values of equilibrium constant for adsorption of both inhibitors were calculated from the intercepts of Fig. 5(a), (b), (c), (d). Calculated values of K_{ads} for all the studied adsorption isotherms are given in Table 2. Largest values of K_{ads} obtained from Langmuir adsorption isotherm for both the inhibitors suggested the strong adsorption of these inhibitors on surface of N80 steel resulting good corrosion inhibition properties for these inhibitors. The equilibrium constant is related with the standard free energy of adsorption (ΔG^0_{ads}) as given below [20]:

$$\Delta G^0_{ads} = -RT \ln(55.5K_{ads}) \quad (7)$$

where R is the gas constant and T is the absolute temperature. The value of 55.5 is the concentration of water in solution in mol L^{-1}. The value of ΔG^0_{ads} was calculated by putting the value of K_{ads} obtained from Langmuir adsorption isotherm in Eq. (7). In general, values of ΔG^0_{ads} up to −20 kJmol^{-1} are related to the physical adsorption, which is electrostatic interaction between the charged inhibitor molecules and the charged metal surface, and those which are more negative than −40 kJmol^{-1} involve chemical adsorption due to charge sharing or charge transfer from the inhibitor molecules to the metal surface [20]. The calculated ΔG^0_{ads} value for BDMA and BDMT was −38.2 and −39.5 kJ mol^{-1}, respectively, at 303 K, which are between the threshold values for physical adsorption and chemical adsorption and closure to −40 kJmol^{-1} indicated that the adsorption process of these inhibitors at N80 steel surface involve both chemical as well as physical adsorption with predominantly the first one [21,22].

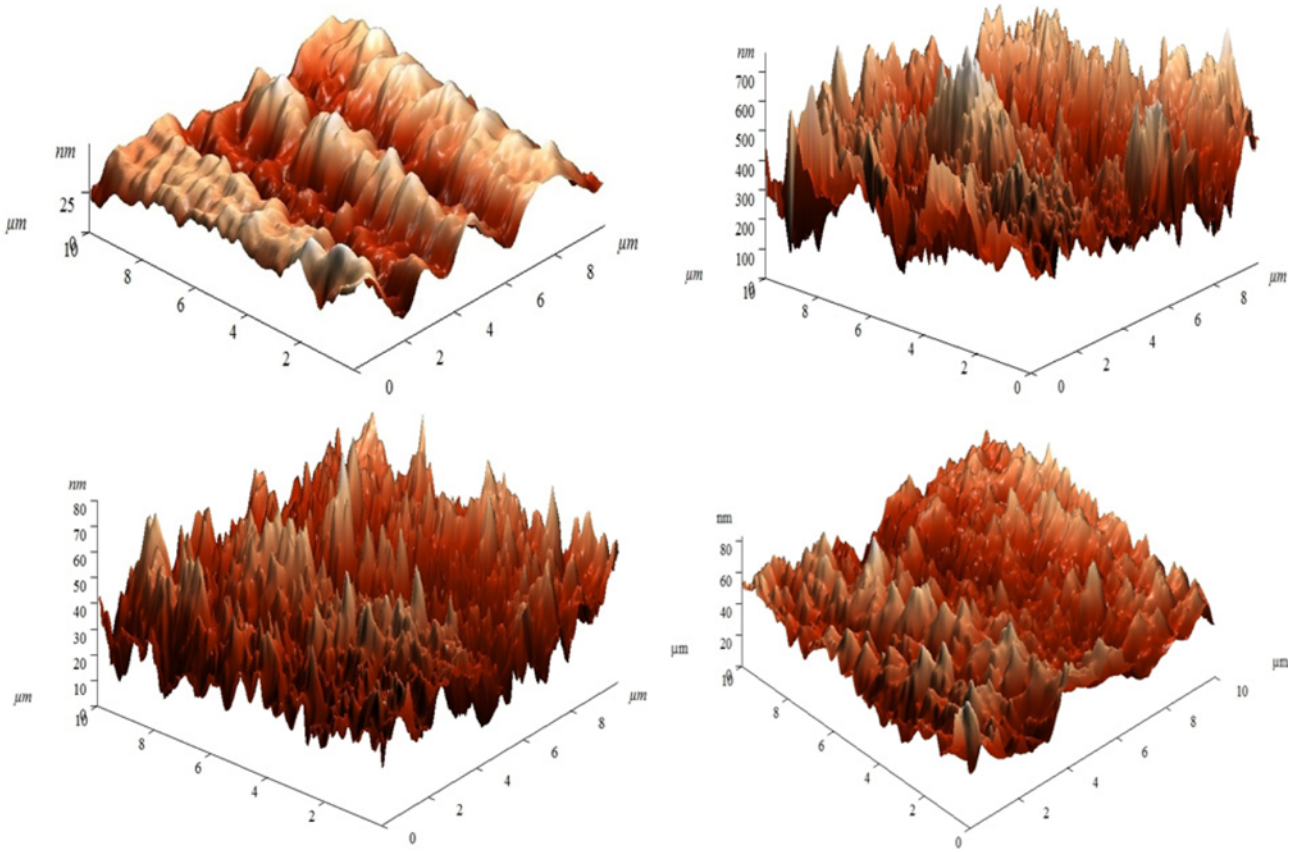

Fig. 6. AFM micrograph of N80 steel surface (a) polished N80 steel (b) Blank in 15% HCl solution (c) with 50 ppm BDMT (d) with 50 ppm BDMA.

4. Atomic Force Microscopy

Three-dimensional AFM images of polished, uninhibited and inhibited N80 samples are shown in Fig. 6(a)-(e). The average roughness of polished N80 steel (Fig. 6(a)) and N80 steel in 15% HCl solution without inhibitor (Fig. 6(b)) was found as 24 and 420 nm. It is clearly shown in Fig. 6(b) that N80 steel sample is damaged due to the acid attack on N80 steel surface. However, in presence of optimum concentration (50 ppm) of BDMT and BDMA as shown in Fig. 6(c), (d), the average roughness was reduced to 42 and 46 nm. The calculated roughness for the BDMT is lower than BDMA reveals that BDMT inhibitor protects the N80 steel surface more efficiently than BDMA form the 15% HCl solution.

5. Theoretical Calculation

The optimized structure, E_{HOMO} and E_{LUMO} of both the inhibitors are shown in Fig. 7(a), (b). The quantum chemical parameters such as the energy of the highest occupied molecular orbital (E_{HOMO}), the energy of the lowest unoccupied molecular orbital (E_{LUMO}), energy gap (ΔE), dipole moment (μ) absolute electronegativity (χ), global hardness (γ) and softness (σ) and fraction of electrons transferred from the inhibitor molecule to the metal surface (ΔN) obtained are summarized in Table 3. The frontier molecular orbital energies (E_{HOMO} and E_{LUMO}) are important parameters for determination of the reactivity of a chemical species. The higher value of E_{HOMO} is associated with the high electron donating ability of a molecule, whereas a lower value of E_{LUMO} suggests that the molecule easily accepts electrons from the donor molecules [23].

For the calculations of quantum chemical parameters such as absolute electronegativity (χ), global hardness (γ) and softness (σ) and fraction of electrons transferred from the inhibitor molecule to the metal surface (ΔN) following equations were used [24].

$$\chi = -\frac{E_{LUMO} + E_{HOMO}}{2} \tag{8}$$

$$\gamma = \frac{E_{LUMO} - E_{HOMO}}{2} \tag{9}$$

$$\sigma = \frac{1}{\gamma} \tag{10}$$

$$\Delta N = \frac{\chi_{Fe} - \chi_{inh}}{2(\gamma_{Fe} + \gamma_{inh})} \tag{11}$$

where a theoretical value of $\chi_{Fe} \approx 4.06$ eV is taken for iron and $\gamma_{Fe} = 0$ is taken assuming that **I=A** for bulk metals [24].

Generally, higher value of ΔN is associated with higher inhibition efficiency of the inhibitor molecule [25]. It was reported previously by some researchers that smaller values of ΔE and higher

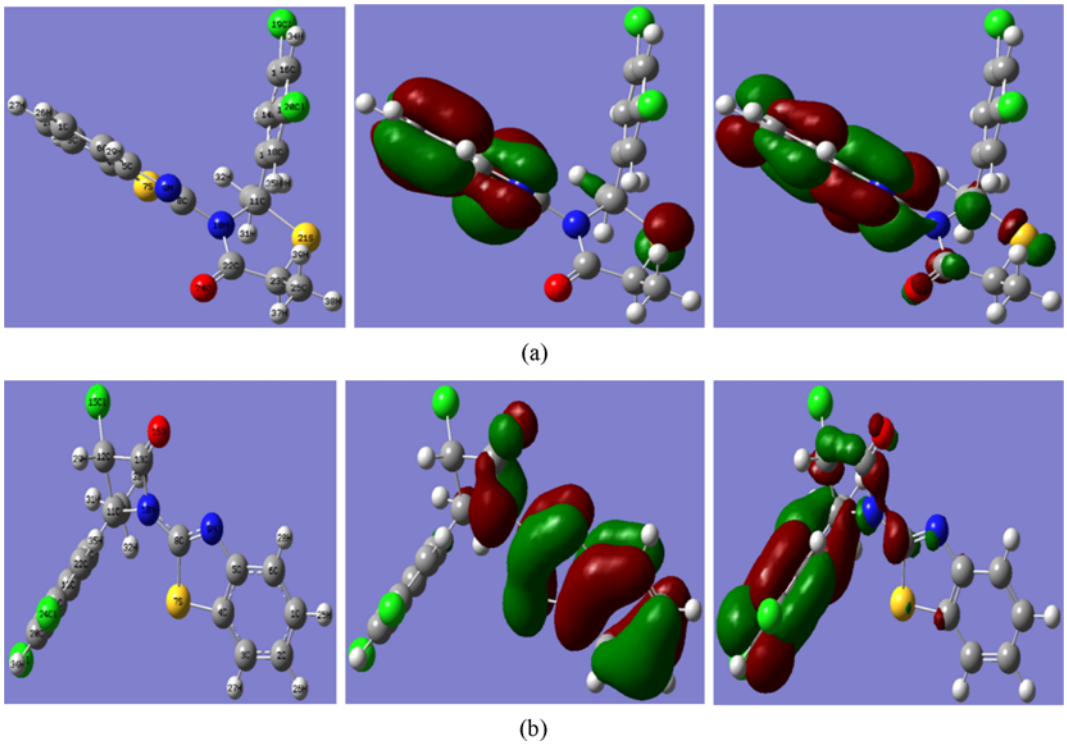

Fig. 7. The optimized structure (left) and HOMO (center) and LUMO (right) distribution for molecules (a) BDMT (b) BDMA [Atom legend: white=H; Grey=C; blue=N; red=O; green=Cl; yellow=S].

Table 3. Quantum chemical parameters for different inhibitors

Inhibitor	E_{HOMO} (eV)	E_{LUMO} (eV)	ΔE (eV)	μ (D)	χ (eV)	γ (eV)	σ (eV^{-1})	ΔN
BDMT	−4.4212	−1.4824	2.9488	3.1248	2.9518	1.4744	0.6782	0.3724
BDMA	−4.9432	−1.2426	3.7006	2.9436	3.0929	1.8503	0.5405	0.2586

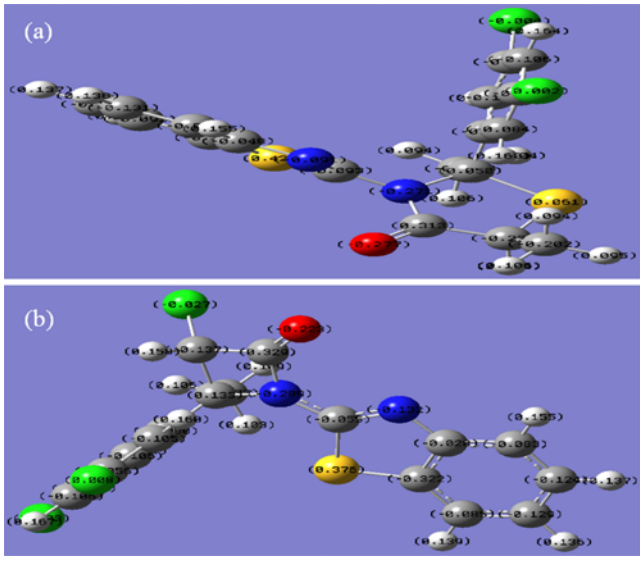

Fig. 8. Mulliken charge density of (a) BDMT (b) BDMA.

values of E_{HOMO}, σ, ΔN and dipole moment (μ) are responsible for enhancement of inhibition efficiency [26]. Thus, the inhibitor BDMT having smaller values of ΔE and higher values of E_{HOMO}, σ, ΔN and dipole moment (μ) (Table 3) than BDMA suggesting that BDMT is more efficient inhibitor than BDMA.

Fig. 7 reveals that the HOMO location in BDMT is mostly distributed in vicinity of the benzothiazole ring and sulfur of thiazolidine ring whereas HOMO location in in BDMA is mostly distributed in vicinity of the benzothiazole ring and oxygen of the azetidine ring. This indicates the reactive sites of the interaction between inhibitor molecules and N80 steel surface. Literature reveals that the use of Mulliken population and HOMO population analysis can be used for the determination of possible adsorption centers of the inhibitors [27-29]. The generalized interpretation given by several authors is that the higher is the magnitude and the number of negatively charged heteroatom present in an inhibitor molecule, the higher is its ability to be adsorbed on the metal surface via a donor-acceptor type bond [27], and the more negatively charged regions with major distribution of the HOMO are also interpreted as possible centers of adsorption. Mulliken charges according to the numeration of corresponding atoms are shown in Fig. 8(a), (b). It is evident from Fig. 8(a), (b) that both inhibitors had a considerable excess of negative charge around the nitrogen, sulfur and oxygen atoms, indicating that these are the coordinating sites of the inhibitors.

CONCLUSIONS

(1) Both BDMA and BDMT act as efficient corrosion inhibitor for N80 steel in 15% HCl solution.

(2) Potentiodynamic polarization studies suggested that both the inhibitors act as mixed-type inhibitors.

(3) The SEM, EDX, AFM and Langmuir adsorption isotherm studies suggested adsorption of inhibitors on N80 steel surface.

(4) Quantum chemical parameters obtained by DFT correlate the experimental results obtained by electrochemical methods.

REFERENCES

1. M. Yadav, D. Behera and U. Sharma, *Corros. Eng. Sci. Technol.*, **48**, 19 (2013).
2. S. Vishwanatham and P. K. Sinha, *Anti-Corros. Methods Mater.*, **56**, 139 (2009).
3. F. Bentiss, B. Mernari, M. Traisnel, H. Vezin and M. Lagrenée, *Corros. Sci.*, **53**, 487 (2011).
4. O. Benali, L. Larabi, M. Traisnel, L. Gengembra and Y. Harek, *Appl. Surf. Sci.*, **253**, 6130 (2007).
5. F. Bentiss, M. Lebrini and M. Lagrenee, *Corros. Sci.*, **47**, 2915 (2005).
6. J. Cruz, R. Martinez, J. Genesca and E. Garcia-Ochoa, *Electroanal. Chem.*, **566**, 111 (2004).
7. K. F. Khaled, *Electrochim. Acta*, **48**, 2493 (2003).
8. K. Mistry and K. R. Desai, *Indian J. Chem.*, **45B**, 1762 (2006).
9. C. Lee, W. Yang and R. G. Parr, *Phys. Rev. B*, **37**, 785 (1988).
10. X. Wang, H. Yang, F. Wang, X. Wang, H. Yang and F. Wang, *Corros. Sci.*, **53**, 113 (2011).
11. W. Li, Q. He, S. Zhang, B. Pei and B. Hou, *J. Appl. Electrochem.*, **38**, 289 (2008).
12. S. Ramesh, S. Rajeswari, *Electrochim. Acta*, **49**, 811 (2004).
13. H. Ashassi-Sorkhabi, B. Shaabani and D. Seifzadeh, *App. Surf. Sci.*, **239**, 154 (2005).
14. S. M. Behpour, N. Ghoreishi, N. Mohammadi and M. Soltani, *Corros. Sci.*, **52**, 4046 (2010).
15. R. Solmaz, G. Kardaş, M. Çulha, B. Yazıcı and M. Erbil, *Electrochim. Acta*, **53**, 5941 (2008).
16. M. Özcan, I. Dehri and M. Erbil, *Appl. Surf. Sci.*, **236**, 155 (2004).
17. M. Lebrini, F. Robert, A. Lecante and C. Roos, *Corros. Sci.*, **53**, 687 (2011).
18. I. Dehri and M. Ozcan, *Mater. Chem. Phys.*, **98**, 316 (2006).
19. S. Ghareba and S. Omanovic, *Electrochim. Acta*, **56**, 3890 (2011).
20. E. Machnikova, K. H. Whitmire and N. Hackerman, *Electrochim. Acta*, **53**, 6024 (2008).
21. R. Solmaz Corros. Sci., **81**, 75 (2014).
22. R. Solmaz Corros. Sci., **79**, 169 (2014).
23. S. Xia, M. Qiu, L. Yu, F. Liu and H. Zhao, *Corros. Sci.*, **50**, 2021 (2008).
24. R. G. Pearson, *Inorg. Chem.*, **27**, 734 (1988).
25. I. Lukovits, E. Klaman and F. Zucchi, *Corrosion*, **57**, 3 (2001).
26. Y. M. Tang, W. Z. Yang, X. S. Yin, Y. Liu, R. Wan and J. T. Wang, *Mater. Chem. Phys.*, **116**, 479 (2009).
27. M. K. Awad, M. R. Mustafa and M. M. Abo-Elnga, *J. Mol. Model.*, **959**, 66 (2010).
28. R. Hasanov, M. Sadikoglu and S. Bilgic, *Appl. Surf. Sci.*, **253**, 3913 (2007).
29. M. A. Amin, K. F. Khaled and S. A. Fadl-Allah, *Corros. Sci.*, **55**, 140 (2010).